Composites Part C: Open Access 10 (2023) 100343

Contents lists available at ScienceDirect

Composites Part C: Open Access

journal homepage: www.sciencedirect.com/journal/composites-part-c-open-access

An automated software development for analysis of the morphological-tensile property relationship in egg shell bio-based particulate composites using machine learning algorithms

G.Elizabeth Rani [a], R. Murugeswari [a], Selvakumar Vairamuthu [b], N. Rajini [c,*], Faruq Mohammad [d], Suchart Siengchin [e], Sikiru O. Ismail [f,*], K. Senthilkumar [g]

[a] Department of Computer Science and Engineering, Kalasalingam Academy of Research and Education, Anand Nagar, Krishnankoil, 626126, India
[b] Engineering Department, University of Technology and applied Sciences-Nizwa, Sultanate of Oman
[c] Department of Mechanical Engineering, Kalasalingam Academy of Research and Education, Anand Nagar, Krishnankoil, 626126, India
[d] Surfactants Research Chair, Department of Chemistry, College of Science, King Saud University, P.O. Box 2455, Riyadh, 11451, Kingdom of Saudi Arabia
[e] Department of Materials and Production Engineering, The Sirindhorn International Thai-German Graduate School of Engineering (TGGS), King Mongkut's University of Technology North Bangkok, 1518 Wongsawang Road, Bangsue, Bangkok, 10800, Thailand
[f] Department of Engineering, School of Physics, Engineering and Computer Science, University of Hertfordshire, Hatfield AL10 9AB, England, United Kingdom
[g] Department of Mechanical Engineering, PSG Institute of Technology and Applied Research, Coimbatore, Tamil Nadu, 641 062, India

ARTICLE INFO

Keywords:
Optical images
Particulate polymeric composites
Image processing
Image analysis software (IAS)

ABSTRACT

This work explored the importance of quantitative observation through imaging methods of optical and electron microscopies on the mechanical properties of particulate polymeric composites. Egg shell powder (ESP) reinforced polypropylene carbonate (PPC) polymeric composites with different filler weight percentage (wt.%) from 1 to 5 wt.% were considered. A cost-effective Image Analysis Software (IAS) was developed to extract black particles from the original optical images. During this process, the optimal image can be reproduced based on its originality by controlling the threshold values from 0.1 to 0.6 in real time situation. Using one-dimensional (1D) Gaussian distribution analysis, the authentication of the particle distribution data was studied and linked to the tensile strength of the composites. The mean value of the particle area collected from the left and right side of the scattered curves has a significant effect on the tensile strength of the composites. The proposed model was validated by comparing the predicted statistical results with the measured tensile strength for different wt.% of ESP composites. From the results obtained, a close agreement of 99% accuracy was observed between the experimental results and the proposed model for the tensile strength of the composites. The innovative study provides more practical and quantitative knowledge on improved particulate polymeric composites, in addition to the detection of failure processes through optical/electron microscopic examination of images. Evidently, the proposed cost effective, accurate and less stressful model can be employed by several composite-based industries to correlate the tensile strengths of particulate polymeric composites with their morphological properties.

1. Introduction

Nowadays, particulate reinforced polymeric composites attract many engineering applications. This is due to their unique characteristics, which include lightweight, ease of manufacturing and eco friendliness. Several studies on particulate polymeric composites have been performed, considering effects of various factors: particle size, distribution, shape for the combination of various particles and polymer system on their mechanical properties. However, prediction of the structure-property relationship from the electron microscopy images has not been explored quantitatively. Hence, this work attempts to establish a common method to quantify the distribution of particles in the polymer matrix and their effects on the tensile properties, using Image Processing Technique (IPT). IPT has gained many attentions among the researchers, due to its cost effectiveness and the scope of providing data according to the user requirement [1]. Using this technology, useful information such as edge detection, contrast, intensity and application of mathematical operations from the images can be retrieved [2,3]. Due

* Corresponding authors.
E-mail addresses: n.rajini@klu.ac.in (N. Rajini), s.ismail3@herts.ac.uk (S.O. Ismail).

https://doi.org/10.1016/j.jcomc.2022.100343

Available online 21 December 2022

to these advantages, the image processing concepts and techniques are widely used in various aspects of fields and sciences. These sectors of application include, but are not limited to, medical science, space science, biological materials, industrial applications and remote sensing [4, 5].

IPT can be applied in all the aforementioned applications, involving various algorithms in machine learning, such as Logistic Regression, Linear Regression, Support Vector Machine (SVM), k-means clustering, Naïve Bayes, K-Nearest Neighbor (KNN), Random Forest etc. [6–9]. Amongst, k-means algorithm is predominantly used in machine learning for different applications, because it is simple, speedy, efficient and suitable for larger datasets [10], as its advantages. Xue et al. [11] investigated into the paleontology microscopic images, using both k-means clustering and SVM algorithms from machine learning. They applied the traditional k-means clustering algorithm for the identification of distribution pattern of images. Szymkowski et al. [12] evaluated the eye retina of human paleontological images, using k-means algorithm. It was mainly focused to separate healthy and unhealthy retinas from dataset. Alnamoly et.al. [13] proposed a newly developed software EG Bio Image to analyze gel electrophoresis images. K-means clustering algorithm was applied to achieve the clustering of groups according to user requirements. However, this software failed to meet the details of calculating the distance between the particles in the clusters, achieving similar coefficients in k-means algorithm and not provided Graphical User Interface (GUI). The k-means algorithm was used in a few studies relevant to skin cancer by means of detecting different patches of skin (color) images and discrimination of skin at the region of interest [14, 15]. Due to the random selection of clusters and failure on achieving proper edge detection, applying the k-means algorithms led to the long-time process and inability to achieve the exact findings from the images. Khairul Islam et al. [16] studied the identification of brain tumor in human body. The concept of principal component analysis (PCA) and k-means algorithm was applied. The image analysis was done by constituting the group of pixels called super pixel, however the clusters were chosen randomly for the purpose of analysis, which failed to provide quantitative information for the larger dataset. Guo et al. [17] applied k-means clustering algorithm to identify landslide susceptibility zonation. The cluster was determined, implying similar pixel values, which resulted to only less susceptibility than natural breaks. Nawaf et al. [18] investigated into the defects and the defect free regions in glass fiber reinforced polymer (GFRP) composites by applying k-means clustering algorithm of machine learning. The centroid for the region of defect and defect free images were calculated, later followed by the distance calculation of two data points, using squared Euclidean distance. Though, there are several studies that leveraged the merits of k-means clustering algorithm, but the application of the same can also be explored further in other area of research. Especially, the parameters include random identification of clusters and measurement of distance between the data points, fixing the centroid and selection of threshold value to choose the optimal images were not used in the of k-means algorithm in machine learning.

Todays, the demand for the development of new materials for several engineering applications is inevitable. Accordingly, the requirement of particles reinforced polymeric composites for lightweight structural applications is very high in many manufacturing sectors [19–21]. The bonding mechanisms between the particle sand polymers were studied, using several characterization methods [22–24]. However, these methods have drawbacks in their usage to investigate the parameters of concern, such as surface topography, chemical components, particle orientation, voids and to mention but a few [25–27]. In general, the use of microscopic techniques is prevalent in the field of material science in order to investigate into the connection between topography and material efficiency [28,29]. Specifically, the optical and scanning electron microcopy images play a crucial role to provide visual observation about the dispersion of particles in the polymer matrix [30–32]. The aforementioned image capturing techniques are used very effectively in the area of particle and fiber reinforced polymer (FRP) composites to predict the failure mechanism, such as crack propagation, interfacial de-bonding and particles pullout, among others [33–36]. Similarly, these techniques were used to provide observations in form of qualitative judgment only, but not exactly in the quantitative aspects.

In addition, several laboratory experiments have been conducted on various particles, as reinforcing materials in polymer matrices [37–39]. These studies focused on the failure mechanisms of fractured composite materials with the aid of a microscopic examination. The usage of the optical processing methods redefined the morphological classification of particulate composites in terms of their individual sizes and forms. The key effect of this imaging method was the resolution of the images produced [40]. The SEM analysis was most suitable for the characterization of nano-sized fillers to understand the dispersion nature of particles, which is the key parameters in deciding the functional properties of the material system [41]. Study on various forms of distributed particles in the bulk polymer matrix, such as uneven distribution has been reported [42]. Patchy distribution and agglomeration of the particulate fillers has been easily observed [43] from the topography of the SEM images. Furthermore, the characteristic of particles was directly related with the interfacial adhesion between the matrix and the filler [44]. The effect of unequal distribution of the particulate filler facilitated poor interfacial adhesion at localized regions, which resulted to lower tensile strength, stress flow, ductility, thermal stability and fatigue has been researched [45]. Eventually, the outputs of all the optimal microscopy images mostly provided only qualitative observations in the field of particulate composites. However, these qualitative observations were sometimes failed to reproduce a similar failure mechanism, which posed a question on the repeatability. Some studies have been reported on the development of a quantitative methodology for analysing the structure of particle reinforced composites, but dealt with analytical modeling [46], X-ray diffraction [47], numerical simulations [48] and image analysis [49].

Hence, this work provided the quantitative analysis on the distribution of particles and their effects on the mechanical properties of particulate polymeric composites, using optical microscopy images. The chicken egg shell powder (ESP) was used as a filler in a film casting and different wt.% of fillers were taken, as inputs for quantitative analysis. Though, various fillers are available, such as starch, polycaprolactone, polyhydroxybutyrate and poly (butylene adipate-co-terephthalate), among others, but ESP is a biodegradable, low cost, an eco-friendly and easily available material. Accordingly, an effort has been made to create user-friendly and cost-effective software with aids of microscopic images as input sources by applying k-means algorithm in machine learning. The aim of using the developed Image Analysis Software (IAS) was to analyze the quantitative information on the distribution of reinforcing fillers in the polymer matrix through microscopic images. A step-by-step simple and systematic approach was used to perform the data processing and *in-situ* statistical analysis. Afterwards, the analytical model was evidently established to correlate the mechanical properties of particulate composites and the data obtained from the statistical study.

2. Methods

Fig. 1 shows the systematic process of developed IAS, where it found the statistical analysis of images for microscopic images. Fig 1 shows the overall process of developed IAS, whereby ESP composite images were taken as inputs, using openCV in Python package deployed in software and set $R = 0$, $G = 0$ and $B = 0$ to extract black particles and applied k-means clustering algorithm to find statistical analysis, as output. In a first step, the microscopic images in any file format, such as JPEG, PNG and/or BMP were the source data directly uploaded into the software, as an input. Initially, the scale bar mentioned in the microscopy image was converted to the number of pixels, which normally can vary image based on the magnification. During this conversion process, each pixel was

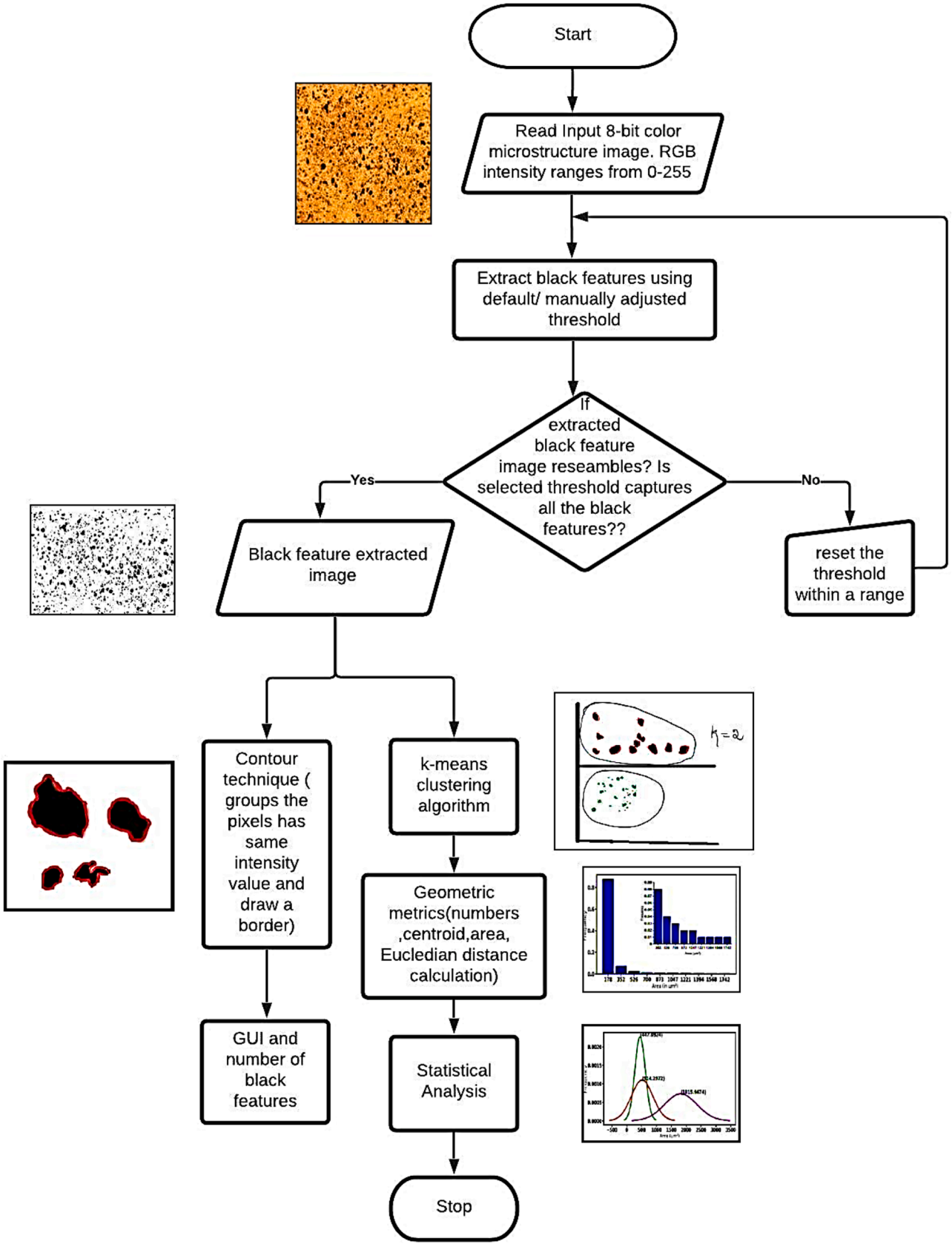

Fig. 1. Step-by-step process of data extraction and statistical analysis, using newly developed IAS.

assumed as square lattice with the length of "a" to cover the area of the scale bar present in the microscopic image. Consequently, the area of the individual pixel was determined from the built-in software. Following this, the actual area of the image can be calculated according to the scale bar appeared in the image.

The area of the image was checked to ensure the reproducibility of the original image from the software before quantifying the data. Afterwards, the size and orientation of the particles were obtained for the different intensity threshold values, ranging between 0.1 and 0.6. The number of particles and their clustering of the converted images can be varied based on the varying threshold values. However, the user has option to identify the best suitable image based on the comparison of mapping between original and the particle extracted images for different threshold values. In this self-developed software tool, a different library packages, such as open computer vision (CV) and Scikit-learn was used to develop automation, starting from the extraction of gray scale particles to statistical analysis. In order to retain the same quality of the images obtained from the microscopic technique, a specific label called dots per inch (dpi) was added as a separate field in the designed software to ensure the verification of image. Similarly, the software can automatically extract the size (height and width) of the original image through the existence of the meta data. Also, this software can automatically operate to find the area of black feature based on the individual pixel value by means of applying grid technique and k-means clustering algorithm in machine learning concepts. Using Python programming concepts, the software was developed.

2.1. Contour technique

Contour technique is a process in which a curve joins all the contour points to accommodate all the pixels inside the boundary. The contour area can be calculated in terms of μm^2, including all the closely packed pixels available in the clusters. The Python coding was used to implement the grid technique, which was described in detail with the help of schematic diagram, as shown in Fig. 2. The following are the steps used in the Python coding to express the concept of grid technique for the irregular contour.

1. Start with any corner node of gray scale particles.
2. To fix single node distance based on the existing calculated gray scale particle size (a).
3. The splitting method is a package inbuilt in Python used to fix the area of the square lattices (a^2 in $\mu m^{2)}$, according to the particle length of a in μm.

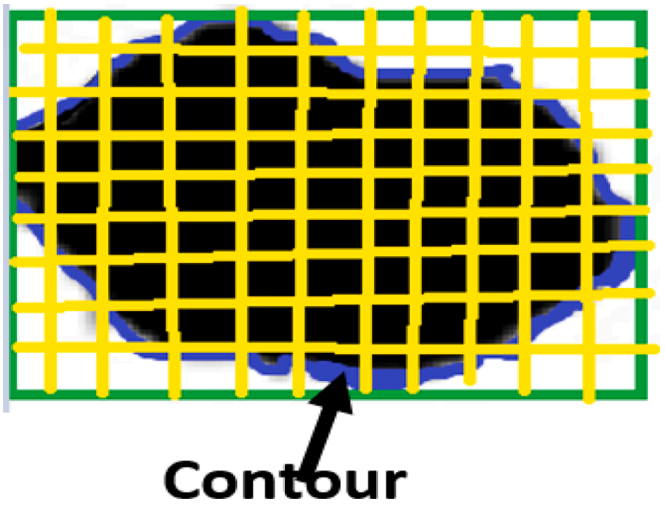

Fig. 2. Schematic diagram of contour and grid technique in single black feature.

4. Repeat the step 3 to obtain equal partition to the whole black features within the contour.

2.2. K-means clustering algorithm

In general, k-means clustering algorithm is used to identify the clusters in any form of images [54]. A modified k-means clustering algorithm was developed with the combination of grid technique and used to extract the gray scale particles in the optical images. Normally, a range of 1–10 clusters can be set in the existing algorithm for a single image. In this modified algorithm, the grid individual particle technique was employed to obtain the means of gray scale particles. Hence, the modified algorithm can increase the productivity through enhanced computational speed of the process. Furthermore, the mean values of the extracted gray scale particles can provide better quantified data [55–57]. To achieve more accurate data processing, the contour technique was applied in each gray scale particle, followed by the implementation of grid technique. This technique can create a rectangle, which was closely bounded in gray scale particles to obtain uniformly distributed grids within the boundary of the cluster. For an example, consider a gray scale particle with the size of 1.15 μm, which can be covered with the square lattice in the size of 1.15 × 1.15 (height and width), using grid technique. The same process can be equally applied to other surrounded particles based on the pixel value for the corresponding case.

Following the grid technique, the modified k-means clustering algorithm available in the machine learning techniques was used in Python coding to obtain more accurate extraction of particles for the distributed reinforcing filler in polymer matrix [58]. A step-by-step process of adopting modified k-means clustering algorithm is subsequently elucidated. In classical k-means clustering algorithm, the user has to find k values by a method, such as elbow and silhouette. A user has to find again and again for correct 'k' clusters. In modified k-means clustering, k values was obtained by the pixel value. The scale bar mentioned in the image can be converted into the number of pixels within the area of scale bar, which can vary based on the magnification of the input images. Each pixel was assumed as square lattice with the length of "a" to cover the area of the scale bar present in the microscopic image. From modified k-means, at initial stage, the user get accurate k values required to form the clusters.

Then, the side of the pixel can be found out, using the following relations, which is inherently built-in software.

The process was carried out by 200 μm scale bar, as a reference for the conversion of one pixel value. For an example, a total number of 105 pixels were obtained to be occupied in the reference scale of 200 μm scale.

2.3. Modified K-means clustering algorithm for finding area of each particle

Input

$M = \{m_1, m_2 \ldots\ldots m_n\}$ // Group of gray scale particle k was calculated from 1 pixel value

1 pixel value = Micron meter scale area / Total pixel presented in specified area k // At initial step the clusters found through IAS software

Output

Assigned $k = 2$ // the number of gray scale feature in a microscopic image

K-means clustering algorithms

Assign initial values for m_1, m_2, m_3, $m_4 \ldots\ldots\ldots m_n$ // gray scale particles in each shape

Repeat

1. n observations of black pixel point into k clusters with nearest mean// black feature values belongs to 1 pixel value = k1 and < black pixel value = k2 (another cluster)

2. put the input symbol in the same group k1 as the closest centroid
3. Measure the Euclidean distance between each input symbol and K centroids
4. Computing new mean for each black feature cluster

Repeat the step 1 to 4 **Until** no reclassification was necessary.

The modified k-means clustering algorithm was unique when compared with the conventional k-means algorithm.

Conventional k-means clustering algorithm has biggest problem, as the clustering outliers are usually far away points and in boundaries points are removed for robust performance. But, the modified k-means clustering algorithm overcame outliers' problem. That is, it included far away pixel point as well as boundary pixel points for quantitative analysis, and none of the pixel values were missed. These clustering outliers can be noted in Fig. 6 right side later, where far away points were also included in statistical computation and the same time, the proposed algorithm is robust. The user needs to spend lot of time in finding k values, using elbow and silhouette. But, here user easily find exact k-values required at minimum time.

3. Sensitivity analysis

To study the operating procedure of the newly developed software, a case study on material was conducted. Accordingly, the polymer composite films reinforced with the ESP in polypropylene carbonate (PPC) polymer were considered. In our previous work [70], mechanical properties of ESP/PPC composite films with varying reinforced fillers of weight percentage (wt.%) of 1, 2, 3, 4 and 5 wt.% were studied. Fig. 3 shows the optical microscopic images of ESP/PPC composite films for varying wt.% of reinforcing filler. The tensile properties of the composite films were analysed with the help of optical microscopic images (Fig. 3), in terms of qualitative observations, such as distribution of particles, orientation and agglomeration [70]. However, the quantitative observation of the ESP dispersion in the PPC matrix was not explored and therefore, it was studied in this current research with the help of newly developed algorithms in the subsequent sections.

According to Fig. 3, the number of ESP particles present in the images progressively increased as the weight percent of fillers increased. Similarly, the ESP particles were randomly orientated in the PPC polymer matrix in all cases. The random distribution of larger number of smaller particles is clearly visible in Figs 3(a-b) when compared with the other wt.%. The number of particles, on the other hand, was substantial in the higher wt.% system, which implied better mechanical properties, such as tensile strength and modulus. Despite the fact that the volume fraction of particles increased with wt.% of filler content, it facilitated the formation of clusters of particles slowly at higher wt.% of filler addition. Furthermore, particle agglomeration was observed from the increase in number of larger particles after filler content of 3 wt.%, which was referred to as a cluster of clusters.

To perform particle quantification and particle clustering, the ESP particles in the polymer matrix were extracted using developed software, as shown in Fig. 4. The extracted particles can change, depending on the intensity threshold that the user selected. Material users must choose the proper threshold value in order to reproduce the particle dispersion shown in the original images. A sample case of addition of 3 wt.% filler to the PPC matrix for various threshold values was obtained to understand the change of particle extraction with regard to threshold value, as shown in Fig. 4. The change of particle counts and dispersion for various intensity thresholds can be readily observed (Fig. 4).

4. Results and discussion

4.1. Optical microscopic images and extraction of particles

Based on the results obtained from this study, a threshold value of 0.45 (Fig. 4e) was observed to reproduce the original picture, as previously shown in Fig. 3(c). More also, Fig. 5 depicts the percentage of variation of number of black dots in the extracted images in comparison with the original images for different threshold intensities, ranging between 0.3 and 0.6. The percentage of variation was observed to decrease as the threshold intensity value increased until it reached 0.4. The minimal variation achieved from the optimum threshold intensity value of 0.45, which exhibited the best mapping of the extracted image with the original. Further increase of threshold value showed the increasing percentage of variation for other two threshold values. From the result of the analysis, it was observed that the threshold intensity value varied case to case, due to the contour required to obtain the black areas.

Furthermore, Fig. 6 left side shows the ESP extracted particles from the optical microscopic images of the varying wt.% of reinforcing filler in PPC polymer matrix for optimal threshold intensity values. In each case, the user can explore the extracted images for the intensity threshold values between 0.3 and 0.6, and it can be compared with the original optical images to find out the optimal selection. The range of threshold can vary based on the particle distribution of different materials obtained from the microscopic technique. Based on visual inspection, the best mapped threshold value was identified as optimal value for the particle wt.%. At higher or more than 3 wt.% of filler reinforced in polymer composite films, the black features were extracted within the threshold range from 0.30 to 0.45 to achieve the maximum percentage of image mapping. On the other hand, the lower wt.% of filler addition produced better mapping only at the high threshold intensities. Nevertheless, the threshold settings helped the extraction of black features in images [50–53] for different 5 wt. composite films. However, the same threshold value cannot be used for all the composite films to extract optimal black features. This was because the presence of gray scale particles varied for different threshold values at different wt.% of composite films, the pixel values was set for black and white, ranging from 0 to 255.

Besides, Fig. 6 right side depicts the normal distribution of the area of the particles in each wt.% of the reinforcing filler. In order to obtain the exact particles distribution, the k-means clustering algorithm came under unsupervised learning category in machine learning used to find out the unlabelled data. All the individual particles present in the images governed by the k-means algorithm could identify k number of centroids, and then cumulated a similar data point to the nearest cluster [59]. Therefore, this study used a newly developed modified k-means algorithms aided to find different range of areas of particles using two different cluster ($k = 2$) mechanism, similar to the reported work [60]. In this approach, grid technique was applied on all the pixels to model as a square lattice having the side of a, which was equivalent to the value of pixel in micron meter [61].

Moving forward, k-means clustering algorithm can be used to fix the cluster and devise a group, covering all related areas of the particles closest to the centroid [62]. Consequently, given the large number of particles placed further from the centroid, the mechanism extended to the next stage. Similarly, the loop replicated in an outward direction before all the usable pixels were converted into the real particle field. Accordingly, the k-means algorithm determined the means of each gray scale particle and created a single cluster. Finally, measurement of the centroids for the clusters was obtained by taking the sum of all the data points of the corresponding cluster. These updated k-means algorithms were extended to all threshold values within the defined range. Topic experts manually pick the acceptable threshold value after the naked eye inspection of the extracted gray scale particle with the original picture of the specific wt.% of the reinforcing filler in the polymer matrix. K-means applied expectation-maximization approach to provide the solution for the issues [63–65]. The expectation-step was used for data points to the nearest cluster and the maximization-step was utilised to measure the centroid of each cluster. Distance-based calculation was adopted to assess the correlation between data points. By using the k-means clustering algorithm, it was convenient to locate the region of each gray scale particle and, in turn, the total black area of the picture was

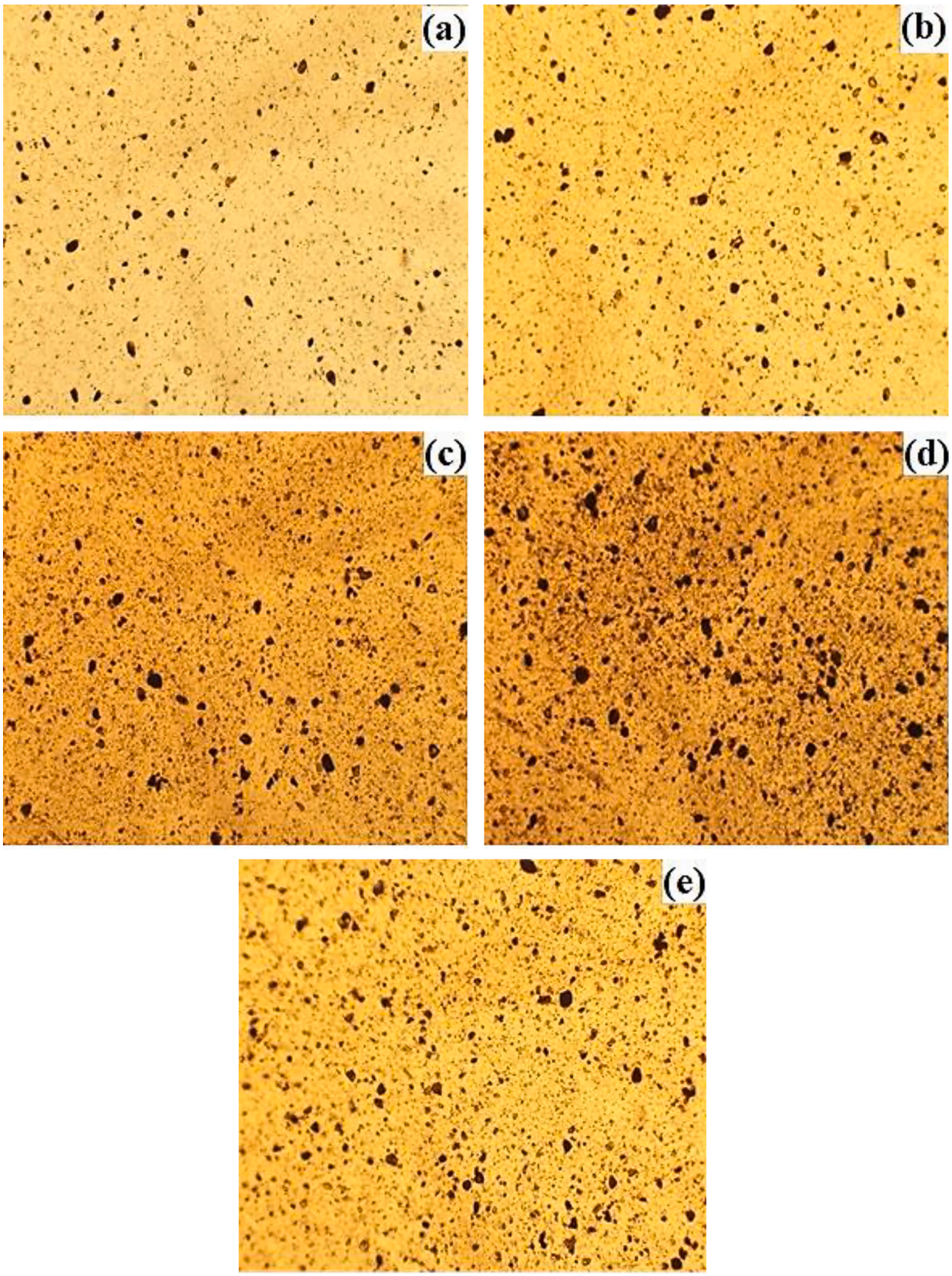

Fig. 3. Optical microscopic images of ESP/PPC composite films with filler contents of (a) 1, (b) 2, (c) 3, (d) 4 and (e) 5 wt.%.

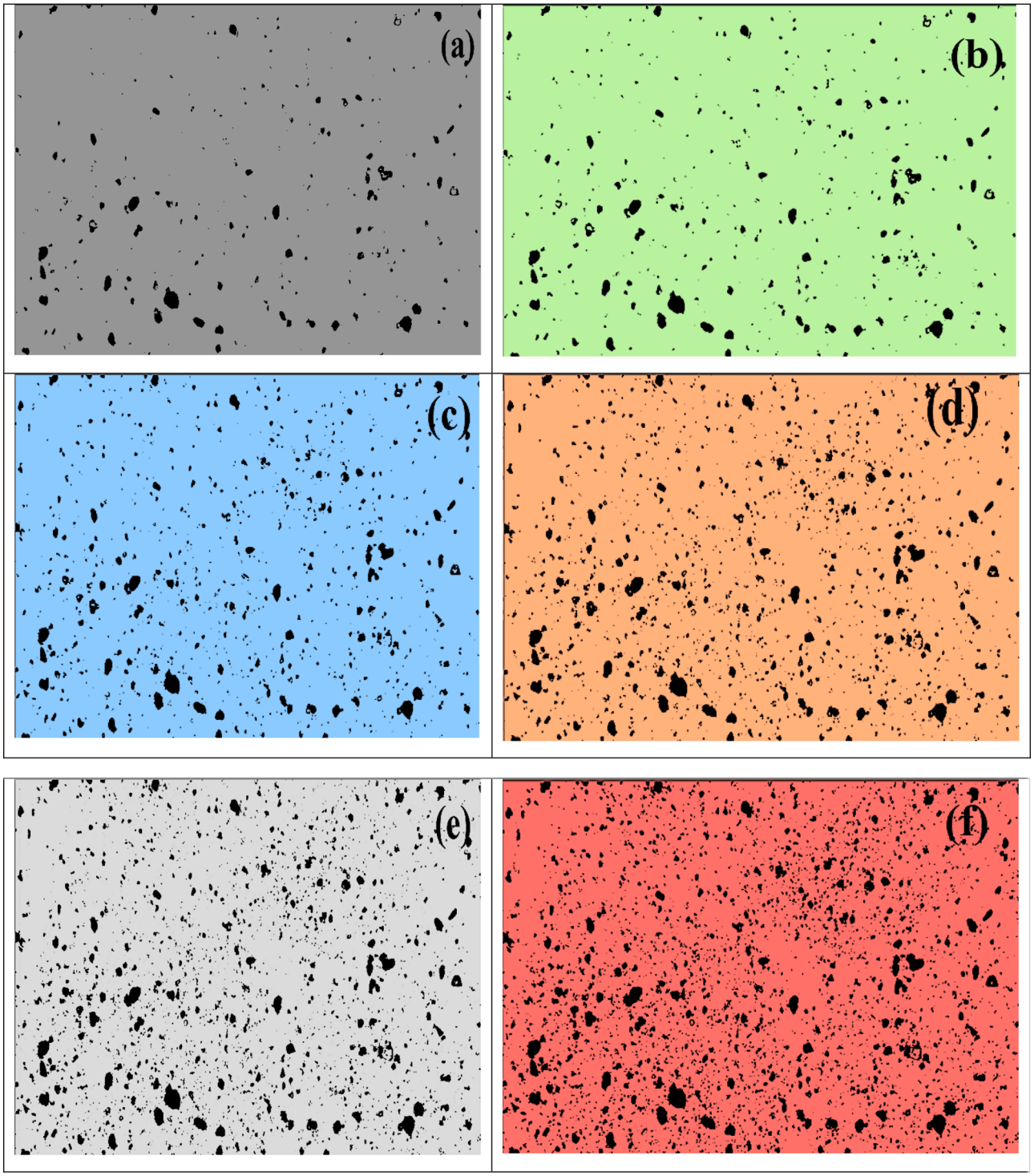

Fig. 4. ESP particle extracted images of 3 wt.% filler reinforced ESP/PPC composite films with varying threshold intensities of (a) 0.30, (b) 0.35, (c) 0.40, (d) 0.45, (e) 0.50 and (f) 0.55.

determined.

Table 1 presents the overall area of the picture considered for this study, which was kept constant in all cases. As a consequence of the study, the area ratio (area of the particles divided by the total area of the image) of the particles for the different wt.% of the composites were observed to be 0.80, 1.50, 7.50, 7.70 and 8.58% for the 1, 2, 3, 4 and 5 wt.%, respectively. A smaller area ratio was reported in the case of lower wt.%, but it was observed to be increased in the case of higher wt.%. However, the higher change in wt.% did not indicate any exponential growth in the percentage of area ratio, instead it appeared to stay stable. This implied that the growing wt.% of particles has overlapping of particles in single positions and consequently, appeared at minimum places than that of lower wt.%. At a lower wt.%, randomly oriented smaller particles were observed, but the appearance of particles in the optical images were exactly reflected in the extracted gray scale particle images to the maximum extent. At the same time, the specified wt.% of the composites cannot be related with the area ratio, since it was difficult to extract the portion of the particles inside the film in the depth

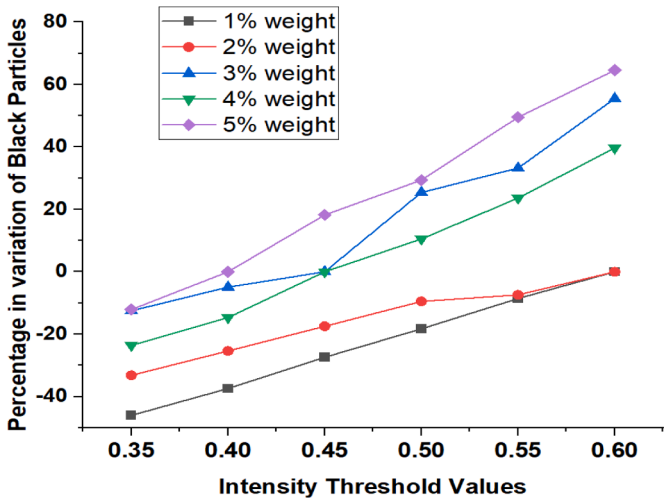

Fig. 5. Histogram plotted for all wt.% of fillers with different threshold values.

direction and overlapping of particles in this surface morphological analysis. Similarly, the region of the particles occupying the images can be expanded by increasing the threshold amount, but the real picture produced from the microscopic technique should be mapped accurately.

4.2. One dimensional Gaussian distribution statistical analysis

In an attempt to establish the validity of the extracted gray scale particle data, one-dimensional (1D) Gaussian normal distribution was obtained, using developed software [66]. Fig. 7 shows the Gaussian distribution for varying filler wt.% from the extracted gray scale particle images. Customized k-means clustering algorithm was used to process Gaussian normal distribution results. Consequently, the results were primarily divided into two clusters dependent on the reference of the centroid values obtained for each cluster [67–69]. Finally, the average values for both the left and the right categories were defined and plotted as a separate distribution. They expressed the importance of all the data derived from the image analysis. The following steps demonstrated a customised k-means clustering algorithm, overseeing the standard distribution of Gaussian.

Using the pre-processing method, which was normalization of results. After standardization, both variables have a common impact on the model, improving the consistency and efficiency of the learning algorithm. Identify the data samples as left and right, using the k-means algorithm (left and right) required specifying the classification number as 2 to reflect these two extreme conditions, including all the gray scale particles in the pictures. Python coding was used to view automated plots for left, right and total mean distribution curves.

From the statistical distribution curve (Fig. 7), it can be easily identified that the left side distribution curves displayed sharp peaks at lower wt.% of the filler distribution up to 4 wt.%, relative to the other wt.%. Similarly, the right-hand curves for these materials displayed a broad peak, owing to a reduced number of larger particles. This implied that the existence of tiny particles was significant when compared with the larger particles up to the reinforcing filler of 4 wt.% in the polymer matrix. On the other hand, the behavior of the left and right-side curves varied with the higher percentage of filler addition. In comparison, there was a considerable number of larger particles in higher wt.%, and the right-side distribution curve often showed relatively sharp peaks.

Table 2 presents the average values of the left and right-side distribution curves for different wt.% of the fillers in the PPC matrix composites. There was a growing trend in average particle area values on both left and the right-side distribution curves. However, the rate of increase in the size of the particles varied between the successive wt.% of the fillers in both distribution curves. The rate of increase of the

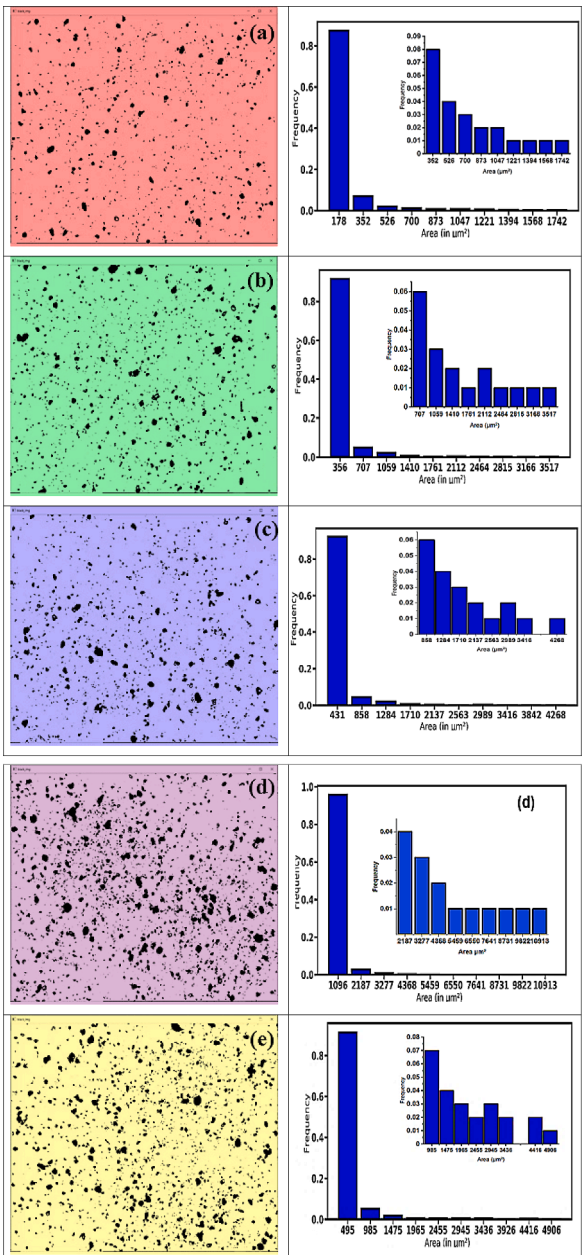

Fig. 6. Left side- ESP extracted particle images obtained from the software for different wt.% of filler with optimal threshold values of (a) 1 wt.% at intensity threshold of 0.6, (b) 2 wt.% at intensity thresholds of 0.6, (c) 3 wt.% at intensity thresholds of 0.45, (d) 4 wt.% at intensity thresholds of 0.45 and (e) 5 wt.% at intensity thresholds of 0.4 and **Right side** - Particle distribution histogram plot for the ESP reinforcing fillers of (a) 1, (b) 2, (c) 3, (d) 4 and (e) 5 wt.% in PPC matrix.

Table 1
Calculation of black feature area for different wt.% in a microscopic image.

Weight percentage (wt.%)	Total area of an image (μm^2)	Calculated black feature area (μm^2)	Total pixel count
1	1,914,556.8	94,954.20	978
2		1,542,96.,12	1214
3		1,838,77.,32	1421
4		3,657,16.,56	1902
5		2,807,53.,44	1509

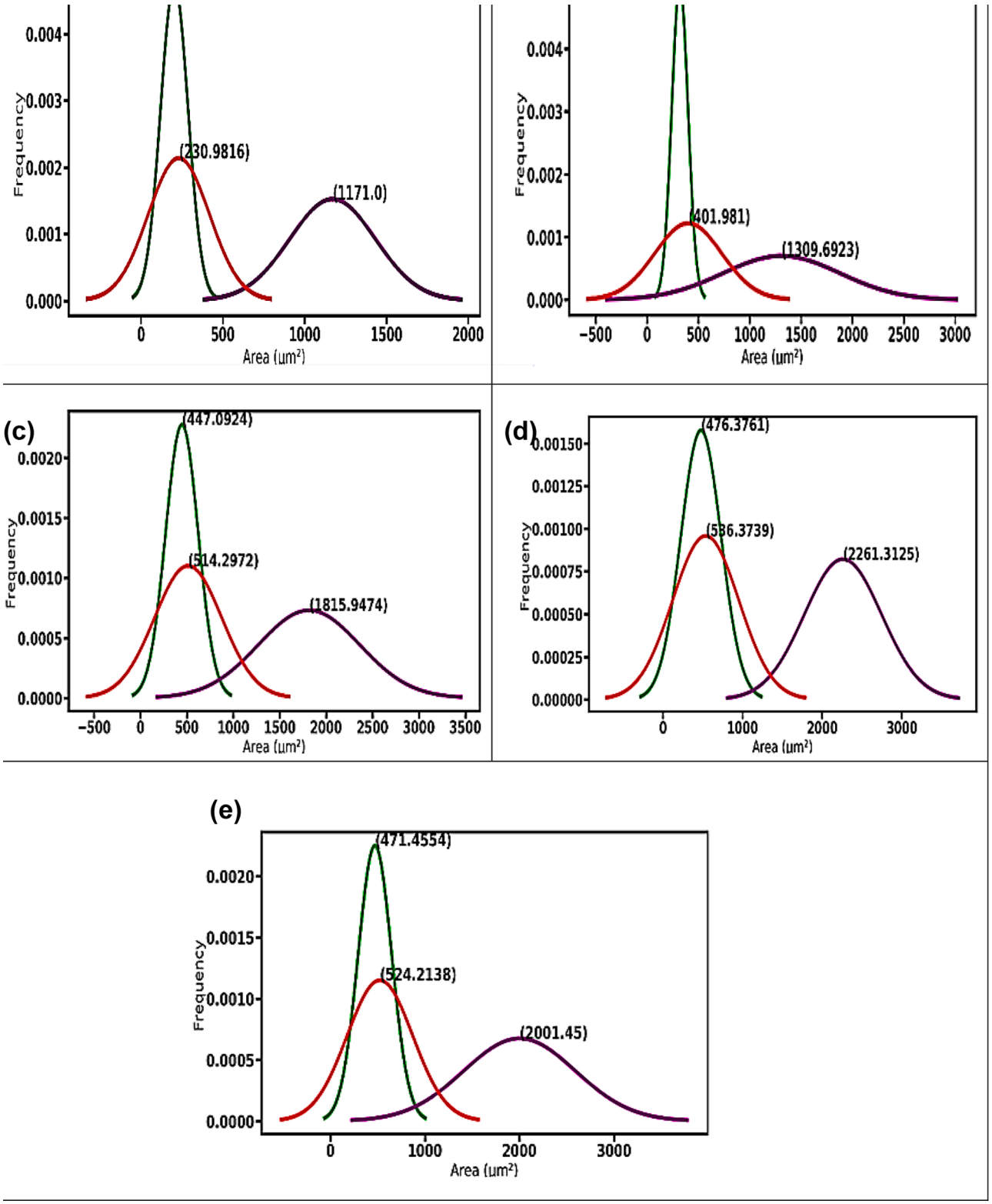

Fig. 7. 1D Gaussian plot distribution for ESP reinforcing filler of 1 to 5 wt.% in PPC polymer matrix.

particle size in the left side curve was flattened after the addition of 3 wt. % filler, but the same was significantly increased for the right-side curves. This phenomenon can be attributed to the agglomeration of the particles, with the addition of a higher wt.%, which could facilitate a coherent adhesion between the particles. Furthermore, the excessive addition of particles could not spread across the system, due to the constraint of the surrounding particles.

It was also observed from the 1D Gaussian distribution curve that there was a small change in the overall mean for increasing wt.% of fillers. It can be deduced that the formation of a particle cluster could be the reason for the change, but it was not very significant.

Table 2
1D Gaussian normal distribution for left and right means.

Weight percentage (wt.%)	Mean value of black particle
1	208.7547
2	403.1531
3	788.2115
4	928.9237
5	1010.8052

4.3. Tensile strength

The experimental investigation of the tensile strengths of the ESP reinforced PPC composites was investigated for differing wt.% of the filler or reinforcement. The results obtained indicated that an improvement in tensile strength was obtained with an increase in wt.% of the filler. At the same time, the rate of increase was decreased after a certain limit or threshold. The decrease in tensile strength can be attributed to the development of agglomerations, as earlier discussed in the literature. Furthermore, there were no objective tests relevant to particle size and distribution.

More also, Table 3 presents the comparison of tensile strengths from experimental results, using proposed technique and model. The model results were tensile properties of ESP reinforced PLA composites, as a function of egg [70], as shown in Fig. 8.

In the derived or predicted model, the tensile strengths of the ESP/PPC composites were correlated with the size and distribution of the particles. The tensile strength values measured from the model were observed to be in good and close agreement with the experimental results. The outcome indicated the visibility of the random direction of the particles of all varying wt.% of the composites. From the data analysis, it was evident that the addition of particles increased the tensile strengths of the composite samples to a threshold loading of 4 wt.%, above which a sudden decrease was observed. Increased particle size was observed with the increasing number of particles apparently noticeable from the declining bandwidth of the right-side normal distribution curve in the statistical study. In comparison, a small change in the average values of the total mean in the Gaussian distribution curve often suggested a rise in particle size, due to the formation of cluster particles.

Furthermore, the increasing pattern was observed up to 4 wt.% of the filler, in excess of which the declining value was observed at 5 wt.%. At a lower range of wt.%, the minimal increase in the number of particles indicated an increased tensile strength value, which means the distribution of smaller particles. On the other side, the slope of the increase in particle size was observed to be high, but the consequence of the same was not substantially expressed in the tensile strength. Around the same period, a small improvement in intensity was observed, which can be attributed to the dispersion of the highest proportion of the minimal size particles in the corresponding wt.% of the filler or reinforcement. After a certain limit at 4 wt.% of the filler, a diminishing pattern was observed in both number of particles and tensile strength plots, as shown in Fig. 9.

The increasing size of the particles after the creation of a cluster can be a reason for the reduction of the number of particles. Additionally, these clusters of particles might have decreased the tensile strength of the composites, due to stress concentrations at the boundary of the agglomerated particles and lack of binding materials between loosely bonded filler materials.

Table 3
Comparision of tensile strengths of experimental results and model.

ESP in the composite (wt.%)	Tensil strength (MPa) Model results	Experimental results
1	17.7 ± 0.4	18.01
2	21.1 ± 0.8	21.50
3	25.5 ± 1.0	26.00
4	30.6 ± 1.7	31.20
5	22.5 ± 0.9	26.30

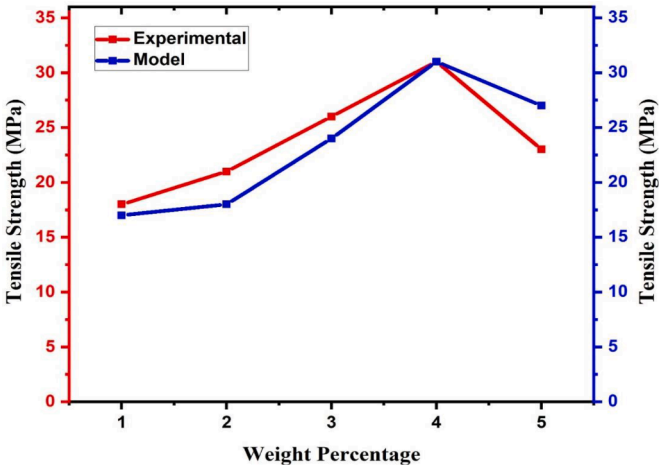

Fig. 8. Comparison of tensile strengths from experimental result and prdicted model.

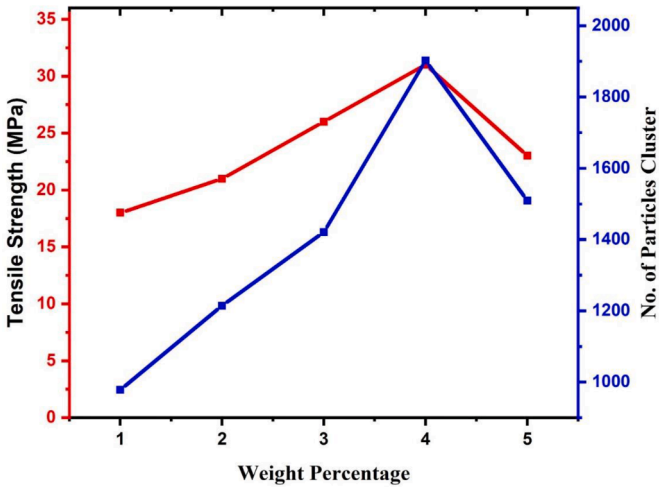

Fig. 9. Comparison between the experimental tensile strengths and the number of particles with increasing wt.% of ESP filler or reinforcement in PPC matrix.

In order to establish the relationship between the wt.% of filler and the statistical parameteres with the tensile strengths of the composites, a linear regression Eq. (1) was derived and solved for the constant coefficients with the coefficiant of correlation, $R = 0.93$ and standard error value as 3.5%.

$$Y = A + BX_1 + CX_2 + DX_3 \quad (1)$$

where A, B, C and D are the constant coefficients and X_1 = weight percentage of filler, X_2 = mean value of the left side Gaussian distribution and X_3 = mean value of the left side Gaussian distribution. The following constant coefficient values were obtained after solving the linear regression equation: $A = 12.639350$, $B = -2.492641$, C = 0.007444 and $D = 0.010012$.

The curve fitting of the linear regression model and the experimental tensile strengths of the ESP/PPC composites with all varying wt.% of the filler followed similar trend. Therefore, the material scientists should be able to estimate the tensile strengths of different particulate composites with any range of wt.%, using the proposed model. However, the influence of random orientation of the particle was not included in this study. This research was entirely based on examination of the region of the size of the particles with reference to the tensile strengths of the composites.

5. Conclusions

A novel IAS has been developed, using Python coding to explore the quantitative observations from the optical imaging technique. The modified k-means clustering algorithm with the combination of grid technique was invented to predict the actual particle size based on the reference scale used in the optimal images. During the process, the extracted particle image was obtained for the optimal threshold value with the maximum percentage of mapping with original image. The 1D Gaussian normal distribution showed two groups of data distributions, according to the size of the particles. An increase in particles size with the wt.% of the fillers was observed from the shifting of total mean towards right.

Also, the statistical analysis established that the left and right mean values for varying wt.% of the fillers were the important parameters, which directly influenced the tensile strengths of the composites. The predicted linear regression model was fitted well with the experimental results, connecting the variables such as filler wt.%, left and right means of the particles size in 1D Gaussian distribution curve. The proposed models closely predicted the values of experimental tensile strengths, and 99% accuracy was obtained.

However, the overlapped particles in the optical images could not be explored from this analysis. Therefore, manufacturers of particle reinforced compounds can only use this derived product and model to gain insight into the correlation between their tensile properties and morphology based on their defined filler wt.%, prior to the real-time practice.

Finally, through the developed software, it was possible to study or find the connection between the structure property and the behavior of the composites, including shape and even particle distribution as well as wt.% at which the agglomeration was formed and suitable wt.% for optimal selection of material with best strength. The proposed technique can be implemented for other composite materials, including glass fiber/polymer, wood, mud bricks, reinforced concrete, to mention but a few.

Data availability

The raw/processed data required to reproduce these results cannot be shared at this time, as the data also form part of an ongoing or further study.

Declaration of Competing Interest

We hereby confirm that this manuscript is an original research work and has not been submitted for publication elsewhere and in any forms.

Data availability

Data will be made available on request.

Acknowledgments

The KSU author extends appreciation to the Deanship of Scientific Research, King Saud University for funding through Vice Deanship of Scientific Research Chairs; Research Chair of Surfactants.

References

[1] W. Yang, L. Zhong, Y. Chen, L. Lin, Z. Lu, S. Liu, Y. Wu, Q. Feng, W. Chen, Predicting CT image from MRI data through feature matching with learned nonlinear local descriptors, IEEE Trans. Med. Image 37 (4) (2018) 977–987.
[2] A.H. Abdel-Gawad, L.A. Said, A.G. Radwan, Optimized edge detection technique for brain tumor detection in MR images, IEEE Access 8 (2020) 136243–136259.
[3] F. Kruggel, A simple measure for acuity in medical images, IEEE Trans. Image Proc. 27 (11) (2018) 5225–5233.
[4] O. Oktay, E. Ferrante, K. Kamnitsas, M. Heinrich, W. Bai, J. Caballero, S.A. Cook, Anatomically constrained neural networks (ACNNs): application to cardiac image enhancement and segmentation, IEEE Trans. Med. Image 37 (2) (2018) 384–395.
[5] Y. Li, D. Liu, H. Li, L. Li, Z. Li, F. Wu, Learning a convolutional neural network for image compact-resolution, IEEE Trans. Image Proc. 28 (3) (2019) 1092–1107.
[6] O. Chatterjee, S. Chakrabartty, Resonant machine learning based on complex growth transform dynamical systems, IEEE Trans. Neural Networks Learn. Syst. 32 (3) (2021) 1289–1303.
[7] W. Xu, W. Li, Granular computing approach to two-way learning based on formal concept analysis in fuzzy datasets, IEEE Trans. Cybernet. 46 (2) (2016) 366–379.
[8] M.-.P. Hosseini, A. Hosseini, K. Ahi, A review on machine learning for EEG signal processing in bioengineering, IEEE Rev. Biomed. Eng. 14 (2020) 204–218.
[9] D. Martens, B.B. Baesens, T. Van Gestel, Decompositional rule extraction from support vector machines by active learning, IEEE Trans. Know. Data Eng. 21 (2) (2009) 178–191.
[10] L. Li, J. Wang, X. Li, Efficiency analysis of machine learning intelligent investment based on k-means algorithm, IEEE Access 8 (2020) 147463–147470.
[11] Y. Xu, Z. Dai, J. Wang, Y. Li, H. Wang, Automatic recognition of palaeobios images under microscope based on machine learning, IEEE Access 8 (2020) 172972–172981.
[12] M. Szymkowski, E. Saeed, M. Omieljanowicz, A. Omieljanowicz, K. Saeed, Z. Mariak, A novelty approach to retina diagnosing using biometric techniques with SVM and clustering algorithms, IEEE Access 8 (2020) 125849–125862.
[13] M.H. Alnamoly, A.M. Alzohairy, I.M. El-Henawy, EGBIOIMAGE: a software tool for gel images analysis and hierarchical clustering, IEEE Access 8 (2020) 10768–10781.
[14] M.Q. Khan, A. Hussain, S.U. Rehman, U. Khan, M. Maqsood, K. Mehmood, Classification of melanoma and nevus in digital images for diagnosis of skin cancer, IEEE Access 7 (2019) 90132–90144.
[15] R. Ashraf, S. Afzal, A.U. Rehman, S. Gul, J. Baber, M. Bakhtyar, I. Mehmood, Oh-young song region-of-interest based transfer learning assisted framework for skin cancer detection, IEEE Access 8 (2020) 147858–147871.
[16] K. Islam, S. Ali, S. Miah, M. Rahman, S. Alam, M.A. Hossain, Brain tumor detection in MR image using superpixels, principal component analysis and template based K-means clustering algorithm, Mach. Learn. Appl. 5 (2021), 100044.
[17] Z. Guo, Y. Shi, F. Huang, X. Fan, J. Huang, Landslide susceptibility zonation method based on C5.0 decision tree and K-means cluster algorithms to improve the efficiency of risk management, Geosci. Front. 12 (6) (2021), 101249.
[18] N.H.M.M. Shrifan, G.N. Jawad, N.A.M. Isa, M.F. Akbar, Microwave nondestructive testing for defect detection in composites based on k-means clustering algorithm, IEEE Access 9 (2020) 4820–4828.
[19] R.M. German, Particulate Composites: Fundamentals and Applications, 1st Ed., Springer Cham/Springer International Publishing, Switzerland, 2016, pp. 1–436.
[20] P.A. Smith, J.A. Yeomans, Benefits of fibre and particulate reinforcement, Mater. Sci. Eng. II (2011) 1–9.
[21] A. Muc, M. Barski, Design of particulate-reinforced composite, Materials (Basel) 11 (2) (2018) 1–20.
[22] X. Qiu, N.H. Tariq, L. Qi, J.-.R. Tang, X.-.Y. Cui, H. Du, J.-.Q. Wanga, T.-.Y. Xiong, Influence of particulate morphology on microstructure and tribological properties of cold sprayed A380/Al2O3 composite coatings, J. Mater. Sci. Technol. 44 (2020) 9–18.
[23] S.H. Lim, S.Y. On, H. Kim, Y.H. Bang, S.S. Kim, Resin impregnation and interfacial adhesion behaviors in carbon fibre/epoxy composites: effects of polymer slip and normalized surface free energy with respect to the sizing agents, Compos. Part A Appl. Sci. Manuf. 146 (2021), 106424.
[24] K. Renner, J. Móczó, G. Vörös, B. Pukánszky, Quantitative determination of interfacial adhesion in composites with strong bonding, Europ. Polym. J. 46 (10) (2010) 2000–2004.
[25] C.J.R. Verbeek, The influence of interfacial adhesion, particle size and size distribution on the predicted mechanical properties of particulate thermoplastic composites, Mater. Lett. 57 (13–14) (2003) 1919–1924.
[26] M. Tanimoto, S. Ando, Prevention of void formation in particulate-filled polymer composites: effects of thermoplastic matrices and residual solvent, Compos. Sci. Technol. 123 (2016) 268–275.
[27] J. Sun, H. Zhang, W. Fan, S. Chen, Automatic acquisition of particle orientation by interferometric out-of-focus image, Optics Comm. 486 (2021), 126795.
[28] H.M. Chethanbabu, M. Ramachandra, Evaluation of mechanical properties of polypropylene fibre reinforced epoxy composite filled with silicon carbide particulates, Mater, Today Proc. 46 (10) (2021) 4400–4406.
[29] A.A. Adediran, F.O. Edoziuno, C.C. Nwaeju, B.U. Odoni, O.S. Adesina, A. Olayanju, Functional and morphological characterization of hybrid particulate reinforced polyester composites,, Mater. Today Proc. 44 (1) (2021) 2813–2819.
[30] A.S. Pareta, R. Gupta, S.K. Panda, Experimental investigation on fly ash particulate reinforcement for property enhancement of PU foam core FRP sandwich composites, Compos. Sci. Technol. 195 (2020), 108207.
[31] S.M. Kumar, R.S. Begum, M. Vasumathi, N.S.K. Ross, Applying visualization techniques to study the fluid flow pattern and the particle distribution in the casting of metal matrix composites, J. Manuf. Proc. 58 (2020) 668–676.
[32] I. Janigová, V. Khunová, J. Kozánková, Plasma treatment of particulate polymer composites for analysis by scanning electron microscopy: I. Morphology of silica filled low density polyethylene, Polym. Test. 18 (1) (1999) 51–61.
[33] I. Jirawattanasomkul, H. Minakawa, S. Likitlersuang, T. Ueda, J.-.G. Dai, N. Wuttiwannasak, N. Kongwang, Use of water hyacinth waste to produce fibre-reinforced polymer composites for concrete confinement: mechanical performance and environmental assessment, J. Clean. Prod. 292 (2021), 126041.

[34] P. Wang, J. Wen, H. Lei, B. Xu, Y. Liu, L. Yang, D. Fang, Morphology characterization and *in-situ* three-dimensional strain field monitor of short carbon fibre-reinforced polymer composites under tension, Compos. Struct. 262 (2021), 113634.
[35] K. Kushimoto, M. Moriyama, A. Shimosaka, Y. Shirakawa, J. Hidaka, S. Ishihara, J. Kano, Measurement method for dispersion states of filler particles in particulate compositematerials by macroscopic permittivity, Adv. Powder Technol. 32 (1) (2021) 272–282.
[36] J. Duan, K.O. Reddy, B. Ashok, J. Cai, L. Zhang, A.V. Rajulu, Effects of spent tea leaf powder on the properties and functions of cellulose green composite films, J. Environ. Chem. Eng. 4 (1) (2016) 440–448.
[37] T.S.M. Kumar, N. Rajini, S. Siengchin, A.V. Rajulu, N. Ayrilmis, Influence of *Musa acuminate* bio-filler on the thermal, mechanical and visco-elastic behavior of poly (propylene) carbonate biocomposites, Int. J. Polym. Analy. Charact. 24 (5) (2019) 439–446.
[38] T.S.M. Kumar, N. Rajini M. Jawaid, A.V. Rajulu, J.T.W. Jappes, Preparation and properties of cellulose/tamarind nut powder green composites (green composite using agricultural waste reinforcement), J. Nat. Fibres 15 (1) (2018) 11–20.
[39] L. Wang, J.Y. Park, Y. Fu, Representation of real particles for DEM simulation using X-ray tomography, Constr. Build. Mater. 21 (2) (2007) 338–346.
[40] deA.M. Pereira-da-Silva, F.A. Ferri, Scanning Electron Microscopy, Nanocharacterization Techniques, Elsevier Inc., 2017, pp. 1–35.
[41] M. Niinomi, Metals For Biomedical Devices, 2nd Ed., Elsevier Woodhead, United Kingdom, 2019.
[42] P. Sivaranjana, E. Nagarajan, N. Rajini, M. Jawaid, A.V. Rajulu, Formulation and characterization of in situ generated copper nanoparticles reinforced cellulose composite films for potential antimicrobial applications, J. Macromol. Sci. Part A Pure Appl. Chem. 55 (1) (2018) 58–65.
[43] P. Sivaranjana, E.R. Nagarajan, N. Rajini, M. Jawaid, A.V. Rajulu, Cellulose nanocomposite films with in situ generated silver nanoparticles using *Cassia alata* leaf extract as a reducing agent, Int. J. Biol. Macromol. 99 (2018) 223–232.
[44] P. Sivaranjana, E.R. Nagarajan, N. Rajini, N. Ayrilmis, A.V. Rajulu, S. Siengchin, Preparation and characterization studies of modified cellulosic textile fabric composite with *in situ*-generated AgNPs coating, J. Ind. Text. (2019) 1–16.
[45] J. Segurado, J. LLorca, Computational micromechanics of composites: the effect of particle spatial distribution, Mech. Mater. 38 (8–10) (2006) 873–883.
[46] P. Kurtyka, N. Rylko, Quantitative analysis of the particles distributions in reinforced composites, Compos. Struct. 182 (2017) 412–419.
[47] Y. Tang, Z. Chen, A. Borbély, G. Ji, S.Y. Zhong, D. Schryvers, V. Jie, H.W. Wang, Quantitative study of particle size distribution in an *in-situ* grown Al–TiB_2 composite by synchrotron X-ray diffraction and electron microscopy, Mater. Charact. 102 (2015) 131–136.
[48] S. Vongehr, S. Tang, X. Meng, Quantitative analysis of particle distributions by comparison with simulations, Microsc. Microanaly. 17 (61–66) (2011) 61–66.
[49] N. Silva1, A. Velhinho, Assessment of particle clustering in MMCs by quantitative image analysis, Mater. Sci. Forum 514-516 (2006) 779–783.
[50] M.J. Muckley, D.C. Noll, J.A. Fessler, Fast parallel MR image reconstruction via b1-based, adaptive restart, iterative soft thresholding algorithms (BARISTA), IEEE Trans. Med. Imag. 34 (2) (2015) 578–588.
[51] C. Rodrigues, Z.M.A. Peixoto, F.M.F. Ferreira, Ultrasound image denoising using wavelet thresholding methods in association with the bilateral filter, IEEE Latin America Trans. 17 (11) (2019) 1800–1807.
[52] N. Eslahi, A. Aghagolzadeh, Compressive sensing image restoration using adaptive curvelet thresholding and nonlocal sparse regularization, IEEE Trans. Image Proc. 25 (7) (2016) 3126–3140.
[53] S.-.C. Pei, C.-.M. Cheng, Color image processing by using binary quaternion-moment-preserving thresholding technique, IEEE Trans. Image Proc. 8 (5) (1999) 614–628.
[54] L. Jia, M. Li, P. Zhang, Y. Wu, H. Zhu, SAR image change detection based on multiple kernel k-means clustering with local-neighborhood information, IEEE Geosci Remote Sens. Lett. 13 (6) (2016) 856–860.
[55] M. Mignotte, Segmentation by fusion of histogram-based k-means clusters in different color spaces, IEEE Trans. Image Proc. 17 (5) (2008) 780–787.
[56] S.N. Sulaiman, N.A.M. Isa, Adaptive fuzzy-K-means clustering algorithm for image segmentation, IEEE Trans. Cons. Elect. 56 (4) (2010) 2661–2668.
[57] L. Liu, Z. Jia, J. Yang, N.K. Kasabov, SAR image change detection based on mathematical morphology and the k-means clustering algorithm, IEEE Access 7 (2019) 43970–43978.
[58] H. Rong, A. Ramirez-Serrano, L. Guan, Y. Gao, Image object extraction based on semantic detection and improved k-means algorithm, IEEE Access 8 (2020) 171129–171139.
[59] H. Yang, H. Peng, J. Zhu, F. Nie, Co-clustering ensemble based on bilateral k-means algorithm, IEEE Access 8 (2020) 51285–51294.
[60] W.-.L. Du, Y. Zhou, J. Zhao, X. Tian, K-means clustering guided generative adversarial networks for SAR-optical image matching, IEEE Access 8 (2020) 217554–217572.
[61] S.M. Joseph, P.S. Sathidevi, A fully automated gridding technique for real composite cDNA microarray images, IEEE Access 8 (2020) 39605–39622.
[62] Z. Lv, T. Liu, C. Shi, J.A. Benediktsson, H. Du, novel land cover change detection method based on k-means clustering and adaptive majority voting using bitemporal remote sensing images, IEEE Access 7 (2019) 34425–34437.
[63] E. Soltanmohammadi, M. Naraghi-Pour blind modulation classification over fading channels using expectation-maximization, IEEE Comm. Lett. 17 (9) (2013) 1692–1695.
[64] H. Fatakdawala, J. Xu, A. Basavanhally, G. Bhanot, S. Ganesan, M. Feldman, J. E. Tomaszewski, Expectation–maximization-driven geodesic active contour with overlap resolution (EMaGACOR): application to lymphocyte segmentation on breast cancer histopathology, IEEE Trans. Biomed. Eng. 57 (7) (2010) 1676–1689.
[65] T. Qiao, Y. Zhang, H. Liu, Non-linear expectation maximization estimator for TDOA localization, IEEE Wire. Comm. Lett. 3 (6) (2014), 637640.
[66] L.S. Fong, Output distributions of capacity-achieving codes for Gaussian multiple access channels IEEE Comm, Lett. 20 (5) (2016) 938–941.
[67] J.D. Valentine, A.E. Rana, Centroid and full-width at half maximum uncertainties of histogrammed data with an underlying Gaussian distribution-the moments method, IEEE Trans. Nucl. Sci. 43 (5) (1996) 2501–2508.
[68] J.-.L. Widlowski, B. Pinty, T. Lavergne, M.M. Verstraete, N. Gobron, Using 1-D models to interpret the reflectance anisotropy of 3-D canopy targets: issues and caveats, IEEE Trans. Geosci. Rem. Sens. 43 (9) (2005) 2008–2017.
[69] P. Pareek, H.D. Nguyen, Gaussian process learning-based probabilistic optimal power flow, IEEE Trans. Power Syst. 36 (1) (2021) 541–544.
[70] B. Ashok, S. Naresh, K. Obi Reddy, K. Madhukar, J. Cai, L. Zhang, A.V. Rajulu, Tensile and thermal properties of poly(lactic acid)/egg shell powder composite films, Int. J. Polym. Analy. Character. 19 (1) (2014) 245–255.